Dalton Transactions

Accepted Manuscript

ROYAL SOCIETY OF CHEMISTRY

www.rsc.org/dalton

Copper and nickel bind via two distinct kinetic mechanisms to a CsoR metalloregulator

Tatiana V. Porto, Michael. T. Wilson and Jonathan A.R. Worrall

School of Biological Sciences, University of Essex, Wivenhoe Park, Colchester, CO4 3SQ, UK.

To whom correspondence should be addressed: Jonathan Worrall, Tel: +44 1206 872095; email: jworrall@essex.ac.uk

TABLE OF CONTENT GRAPHIC

Copper and nickel ion binding to a bacterial metalloregulator from the copper sensitive operon repressor (CsoR) family are shown to have kinetically distinct mechanisms.

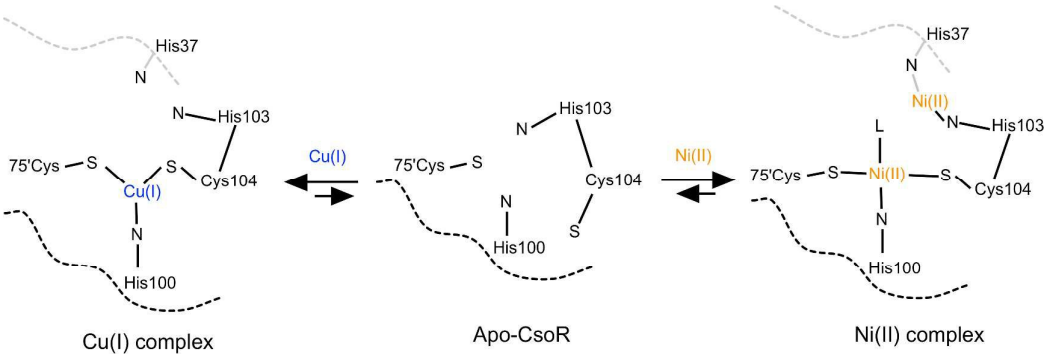

ABSTRACT

The intricate interplay between polypeptide and metal ion binding underscores many of life's fundamental processes. Metalloregulators recognise and bind cognate metal ions during cellular metal stress, evoking a transcriptional response so as to maintain metal ion homeostasis. Members of the copper sensitive operon repressor (CsoR) family of metalloregulators bind to their operator DNA in the absence of a bound metal ion, but on binding Cu(I) an allosteric conformational switch is induced that causes dissociation of the bound DNA. Other divalent metal ions are capable of binding to CsoR members but do not induce the allosteric response observed with Cu(I). The thermodynamics of Cu(I) binding has been studied in this family of metalloregulators, but the binding kinetics and mechanism of Cu(I) or a non-cognate metal ion is unknown. In the present study we have used stopped-flow absorbance kinetics and site-directed variants of the CsoR from *Streptomyces lividans* to monitor binding of Cu(I) and non-cognate Ni(II). The variants have been designed to individually replace known metal ion binding ligands and also to test the role of a histidine residue (His103) close, but not considered part of the Cu(I) first coordination sphere. Cu(I)/Ni(II) ion displacement studies have also been investigated. The kinetic data are most consistent with the existence of two distinct mechanisms that account for Cu(I) and Ni(II) ion binding to this CsoR. In particular Ni(II) has two binding sites; one that has identical amino acid coordination as the Cu(I) binding site and the second involving His103, a residue determined here not to be involved in the mechanism of Cu(I) binding.

INTRODUCTION

In bacteria, metal ion homeostasis and resistance is regulated by the expression of genes under the control of metalloregulators [1-4]. This class of protein binds cognate metal ions with affinities ranging between micro- to zeptomolar [5], triggering an allosteric conformational change, which can inhibit or activate operator DNA binding or enhance transcriptional activation [3]. The CsoR/RncR family of metalloregulators contains members that are metal-responsive repressors of genes that are often part of an operon containing at least one metal-effluxer [3]. A number of metal-sensing CsoR/RcnR members have been characterized. In *Escherichia coli*, RcnR is a Ni(II) and Co(II) responsive repressor of expression of the RcnA Ni(II) and Co(II) efflux-protein [6-8]. InrS is a Ni(II) responsive repressor of the last gene in the *nrs* Ni(II)-efflux operon in *Synechocystis* PCC 6803 [9, 10]. CsoR is widespread across bacteria and is a Cu(I) responsive repressor of the expression of Cu(I)-efflux systems [11]. Structural studies have provided a number of CsoR structures in the apo- [12, 13] and Cu(I)-bound states [11, 14]. These reveal disc-shaped D_2-symmetric homotetramer assemblies with each CsoR protomer consisting of three α-helices of varying lengths (Figure 1A). No structures of RcnR or InrS have so far been reported, but they are considered to be similar to CsoR. In some bacteria a parlog of CsoR has been identified and denoted CstR (CsoR-sulfurtransferase repressor), which does not form a stable complex with a transition metal but acts as a persulfide and polysulfide-regulated repressor [15-17].

A sequence fingerprint, designated W-X-Y-Z, has been used to classify the different sub-families of the metal binding members of the CsoR/RcnR family (Figure 1B and C) [8]. For CsoR the Cu(I) ion binds to the Cys, His and Cys residues of the X-Y-Z fingerprint motif in a favoured trigonal planar geometry [11, 14]. For RcnR and InrS, metal binding residues are retained at the X-Y-Z positions (Figure 1C) [8, 10, 18]. The His at the W position in RcnR and InrS is proposed to provide additional ligation to Ni(II) or Co(II), both of which favour a higher coordination number geometry compared to Cu(I) [10, 19]. The W position is predicted to be located in a sequence region before the start of the N-terminal α1-helix in these proteins. In CsoR this region is considered dynamic, but a recent Cu(I)-bound structure of a CsoR from *Geobacillus thermodenitrificans* reveals that part of its N-terminal region is folded and lies over the Cu(I) binding site [14]. Despite the absence of a metal ion coordinating residue at the W position in Cu(I)-CsoR members, the CsoR from *Bacillus subtilis* has been

shown to coordinate Ni(II), Co(II) and Zn(II) [20]. Binding to higher coordination number metals does not however drive an allosteric response *in vitro* (*i.e.* derepression of operator DNA), demonstrating that the cognate metal ion coordination geometry is critical for allosteric function [20]. Similarly for RcnR, changing the coordination number of the Ni(II) ion form six to four abrogates Ni(II)-sensing [8]. In contrast, InrS has been shown to accommodate a number of different metal ions with varying coordination geometries and still retain the ability to drive allosteric function *in vitro* and *in vivo* suggesting promiscuity in the mechanism of allosteric regulation in InrS not apparent in CsoR or RcnR [18]. Phylogenetic analysis of CsoR/RncR proteins has revealed that the Cu(I)-sensing CsoRs are distributed in four out of seven distinct clades (I, III, IV and VI) [14]. Multiple sequence analysis of CsoRs within each clade indicates that the major features that distinguish the CsoRs in the different groups lie outside the X-Y-Z fingerprint motif [14]. Thus raising the possibility that the mechanism of Cu(I)-allosteric negative regulation of DNA binding may differ between clades [14].

The bacterial cytosol is a metal-controlled environment in which the actions of metalloregulators help to maintain the buffered metal ion concentration [4, 5]. Fluctuation in the set-metal concentration of the cytosol leads to the initiation of a response from the appropriate metalloregulator. For CsoR this would be the binding of Cu(I), which is likely to occur through an associative metal-exchange from labile metal sites present in a Cu chaperone or from the myriad components of a polydisperse buffer [4, 5]. A recent study with the clade III CsoR from *Streptomyces lividans* has demonstrated that an associative metal-exchange mechanism involving the transfer of Cu(I) from a CopZ-like metallochaperone to the CsoR can occur *in vitro* [21]. Based on their ionization and structural properties the two Cys residues of the X-Y-Z-fingerprint of CsoR have considerable nucelophilic properties at physiological pH instigating unidirectional Cu(I) transfer via a ligand-exchange mechanism from CopZ to the CsoR [21]. Whether there is a preference for an initial attack by one of the CsoR Cys residues on the Cu(I) ion bound to the CopZ chaperone is not known.

To gain further insight into metal ion binding in this family of metalloregulators we have used stopped-flow absorbance spectroscopy to investigate the kinetics of Cu(I) binding to CsoR from *S. lividans* as well as the kinetics of a non-cognate metal ion, Ni(II). Elucidation of a binding mechanism for the cognate and non-cognate metals has been aided by site-directed Ala variants of the amino acids at

the individual X-Y-Z positions in the fingerprint region, along with a variant (H103A) that is outside of the fingerprint motif. His103 is shown to play a key role in the kinetics of Ni(II) binding but not for Cu(I) binding. Furthermore, metal displacement studies reveal that Ni(II) has two binding sites, one that utilizes the X-Y-Z fingerprint ligands and the second involving His103.

EXPERIMENTAL

Site-directed mutagenesis of S. lividans CsoR

Site-directed variants (H103A and C104A) were constructed using a method based on Stratagene's Quikchange mutagenesis protocol. The forward and reverse mutagenic primers (nucleotide changes lower case) used to introduce the respective mutations were as follows: H103A forward-5'-GAGCACCTGCGCgcCTGCGTCGCC-3', reverse-5'- GGCGACGCAGgcGCGCAGGTGCTC-3': C104A forward-5'-CACCTGCGCCACgcCGTCGCCGAC-3', reverse 5'-GTCGGCGACGgcGTGGCGCAGGTG-3'. A PCR mix consisting of the pET28a plasmid (0.5 ng/µl) containing the full-length *S. lividans* CsoR gene, the desired mutagenic primers (2.5 ng/µl), Pfu Turbo polymerase and buffer (Agilent), dNTPs (0.2 mM, Fermentas) and DMSO (6 %) to give a final volume of 30 µl was prepared and PCR carried out as follows: 95 ^{o}C (3 min), [95 ^{o}C (1 min), 58 ^{o}C (30 s), 68 ^{o}C (8 min)] x 15, 72 ^{o}C (15 min). Mutant clones were sequenced to corroborate that the intended nucleotide changes were successfully introduced.

Over-expression and purification of S. lividans CsoR and mutants

Wild-type (WT) CsoR and the C75A, H100A, H103A and C104A variants were over-expressed in *Escherichia coli* BL21(DE3) cells and purified as previously described [13]. All purified mutants were folded as deemed from far UV-CD spectroscopy (data not shown).

Protein and metal ion preparation

Concentration of protein samples was determined by UV-Vis spectroscopy (Cary50 spectrophotometer) using an extinction coefficient (ε) for the CsoR monomer at 280 nm of 3105 M^{-1} cm^{-1}. Exchange into the required buffer was carried out using a PD-10 column (GE-Healthcare) pre-equilibrated in the desired buffer. Free thiol content

was determined by the reduction of 5,5'-dithiobis(2-nitrobenzoic) acid (DTNB) monitored at 412 nm (ε = 13 500 M^{-1} cm^{-1}) [22] prior to metal binding studies with average protein:thiol ratios of 1:2 consistently being determined. Stock (1 M) Cu(II)SO_4 (Sigma) and Ni(II)SO_4 (Sigma) solutions were prepared aerobically in de-ionised water. CuCl was prepared in an anaerobic chamber (DW Scientific [O_2] < 2 ppm) and the concentration determined spectrophotometrically by step-wise addition to a known concentration of the Cu(I)-specific bidentate chelator bicinchoninic acid (BCA) (Sigma) using an ε at 562 nm of 7900 M^{-1} cm^{-1} for $[Cu^{I}(BCA)_2]^{3-}$ [23]. Cu(I)-CsoR was prepared by the stoichiometric addition of CuCl in the anaerobic chamber and removed for stopped-flow studies in a gas tight syringe (Hamilton).

Electrophoretic mobility shift assay (EMSA)

DNA oligomers (Sigma) were prepared in 10 mM HEPES pH 7.5, 150 mM NaCl. Concentrations of individual oligonucleotides were determined using appropriate extinction coefficients at 260 nm on a Nanodrop2000 (Thermo Scientific). Equal concentrations of complementary strands were annealed by heating to 96 ^{o}C in a water bath for 5 min and then left to incubate to room temperature over-night. Samples for analysis by EMSA were all prepared in 10 mM HEPES pH 7.5, 150 mM NaCl, 1 mM DTT under anaerobic conditions and consisted of 0.5 μM of DNA duplex, 0.5 μM of DNA incubated with 4 μM WT CsoR monomer and 0.5 μM of DNA incubated with 4 μM WT CsoR monomer followed by addition of either excess Cu(I) or Ni(II). All samples were loaded (20 μl) to a pre-run 6% Tris-Borate EDTA (TBE) polyacrylamide gel. Gels were stained for 30 min in an ethidium bromide solution followed by imaging.

Anaerobic procedures

Anaerobic buffers were prepared by repeated exposure to vacuum followed by equilibration with oxygen free argon. Buffers were taken into glass syringes equipped with coupling tubes allowing dilutions of Cu(I) solutions without exposure to air. Protein solutions were prepared by similar cycles of gentle degassing and equilibration with oxygen free argon. The stopped-flow apparatus was washed through with anaerobic buffer prior to introduction of the reactants (protein and Cu(I))

under study. This procedure permits reactions to be studied at oxygen concentrations of 2 μM or below.

Stopped-flow spectroscopy

Kinetic experiments were carried out using an Applied Photophysics (Leatherhead, UK) SX20 stopped-flow spectrophotometer equipped either with a photomultiplier detection system (for measurements at 300 nm) or with a diode array attachment capable of taking spectra at 3 ms intervals thermostatted at 20 ^{o}C with a Peltier system. At wavelengths below 360 nm a combination of lamp and diode sensitivity lead to an attenuation of the measured absorbance. This becomes most noticeable as the wavelength decreases and leads to a distortion in the peak position in absorption spectra in this region. The consequence of this is that the absorption band centered at 340 nm appears at 350 nm and accounts for an apparent discrepancy between the static and diode array kinetic spectrometers. All proteins were prepared in anaerobic 20 mM HEPES pH 7.4, 50 mM NaCl (see above) and diluted to give final concentrations of 20 μM (10 μM after stopped-flow mixing). The protein was mixed with Cu(I) or Ni(II) with the respective protein in the concentration ranges (after mixing) of 34-137 μM and 50-800 μM, respectively. For the Cu(I) binding experiments and displacement studies anaerobic conditions were employed. Single time courses captured using the photomultiplier system were averaged (n = 5) and fitted to the sum of exponentials (two or three). Global analysis of the full spectra data was accomplished using the ProK programe (Applied Photophysics, Leatherhead UK) that employs singular value decomposition (SVD) to determine the number of independent spectral components comprising the data set and also allows fitting to specific kinetic models, in this case a simple sequential mechanism described by the Bateman equation [24]. The rate constants reported are an average of triplicate experiments carried out on different days and with different protein batches.

RESULTS AND DISCUSSION

The kinetics of Cu(I) binding to CsoR and variants

Binding of Cu(I) to WT CsoR under anaerobic conditions was monitored at 250 nm using a stopped-flow spectrometer. Representative time courses with increasing Cu(I) concentrations are illustrated in Figure 2A. A very rapid phase occupying the first 5-

10 ms after mixing is followed by a slower phase taking around 1 s to complete (Figure 2A). The time courses, however, were best fitted to a three component exponential function as judged by the random distribution of residuals, which was not seen for a two-exponential fit. This fitting procedure gave rate constants for a fast (k_{1Cu}), and two slower phases (k_{2Cu} and k_{3Cu}), with the third phase comprising less than 10 % of the total amplitude change at 250 nm. For all phases the pseudo first-order rate constants were independent of [Cu(I)] between 5 and 100 μM of Cu(I) with the average across the concentration range reported in Table 1. The total amplitude change for the transition as a function of [Cu(I)]/[CsoR monomer] reveals a linear relationship until a break point is reached at a stoichiometry of ~ 1:1, indicative of a high affinity Cu(I) binding process (Figure 2B). This stoichiometry is consistent with previously reported titration experiments, where changes in the absorption spectrum at 240 nm, indicative of Cu(I)-thiolate bond formation, was monitored [13].

The kinetics of Cu(I) binding to the H103A variant and the X-Y-Z fingerprint variants were next investigated. His103 is relatively well conserved amongst clade III and IV Cu(I)-CsoR members and is located between the Y (His100) and Z (Cys104) fingerprint residues. Structural data has revealed that, in the apo-form of *S. lividans* CsoR the imidazole ring of His103 lies in an orientation that together with His100 and Cys75' could conceivable lead to participation in metal ion coordination [13] (Figure 1B). Stopped-flow experiments with the H103A variant gave essentially identical Cu(I) concentration independent rates (Table 1), total amplitude change and stoichiometry of Cu(I) binding as WT CsoR. This implies that His103 is not involved in the Cu(I) binding process under investigation. However, differences are apparent for the X-Y-Z fingerprint variants. For C75A the rate constants remain the same as WT (Table 1), but the [Cu(I)] required to reach full saturation (*i.e.* to give the same amplitude change as for the WT) increases (Figure 2C). This suggests a weaker affinity for Cu(I) in the absence of Cys75' and enables for a fit to the data to yield a K_d = 11 (2) μM (Figure 2C inset). For the C104A variant the kinetics and rate constants are largely unaffected (Table 1), but the total amplitude change at Cu(I) saturation is now ~ 35 % of the WT (Table 1) despite a 1:1 stoichiometry being retained. Likewise, the total amplitude change at Cu(I) saturation for the H100A variant also decreases to ~ 60 % of the WT (Table 1), with a 1:1 stoichiometry of binding maintained. Therefore the H100 and C104 residues of the X-Y-Z motif are

seemingly important to develop the full absorbance change at 250 nm on Cu(I) binding. These data along with those from the WT suggest the observed kinetic phases are not reporting the initial binding of Cu(I) as there is no dependence of the rate constants on [Cu(I)]. Instead a post-binding event is likely being monitored that reports rearrangement(s) of the metal binding site once Cu(I) is bound. Initial binding must therefore be optically silent and must be faster than the rates of the fastest process with a second order binding rate constant > 10^7 $M^{-1}s^{-1}$.

Ni(II) binding to CsoR and variants

Addition of Ni(II) to WT CsoR generates metal-dependent spectral features at 275 nm and 340 nm in the absorption spectrum (Figure 3A). The spectrum is reminiscent of *B. subtilis* Ni(II)-CsoR [20] and Ni(II)-InrS [10], where the bands at 340 nm and 333 nm, respectively, have been assigned as ligand to metal charge transfers (LMCT) arising from Ni(II)-thiolate bonds. Both spectral bands saturate on binding 1 equivalent of Ni(II), indicating a high affinity binding process. In contrast the absorbance band at 340 nm for *S. lividans* CsoR does not saturate at 1 equivalent of Ni(II) and displays a more complex binding isotherm (Figure 3A inset). Based on the tetrameric structure of CsoR the possibility exists that this is a manifestation of cooperativity. However, we rule this out based on the calculation of a Hill coefficient of > 4 for a sigmoidal fit to the data. The alternative explanation is the existence of at least two binding sites for Ni(II) with different affinities and optical properties (*vide infra*). A very weak transition at ~ 480 nm is observed at saturating [Ni(II)] in the WT absorption spectrum. This has been attributed in Ni(II)-InrS and *B. subtilis* Ni(II)-CsoR to arise from d-d transitions that are consistent with the Ni(II) ion being in a square planar or distorted tetrahedral geometry [10, 20]. The H103A variant gives an identical absorption spectrum to that of WT CsoR upon addition of saturating Ni(II). However, the 340 nm band displays a simpler complex binding isotherm compared to WT CsoR. By contrast the 340 nm band is very weak in all the X-Y-Z fingerprint variants in the presence of saturating Ni(II). This illustrates that the previously proposed 340 nm Ni(II)-thiolate LMCT band is not only sensitive to the Cys residues at the X and Z positions, but also to the coordinating residue at the Y position (His100) of the fingerprint (Figure 3B). From an EMSA experiment the binding of Ni(II) to WT CsoR pre-incubated with *csoR* operator DNA does not induce the allosteric response observed with Cu(I) (Figure 3C). This is consistent with a previous report for *B.*

subtilis CsoR [20] and reinforces the view that the cognate metal coordination geometry regulates the allosteric response in Cu(I)-CsoR members.

The kinetics of Ni(II) binding to CsoR and variants

Upon rapid mixing of WT CsoR with excess Ni(II) a band at 350 nm rapidly developed (Figure 4A). This is consistent with the observation of the band at 340 nm in the static absorption spectrum (Figure 3A), with the 10 nm offset observed in the stopped-flow (see Materials and Methods). The time courses observed at all wavelengths examined indicated a short "lag-phase" occupying the first few seconds but thereafter (> 90 % of the total amplitude change) could be fitted well by a single exponential (Figure 4B). Analysis of the data using SVD demonstrated that no spectral distinct intermediates occur in this process. No [Ni(II)] dependence was observed over the concentration used (20-800 μM) on the rate (k_{Ni}), implying that, at the time of the first observation, Ni(II) is already bound (Table 2). Furthermore, the total amplitude change plotted as a function of [Ni(II)/[CsoR monomer] indicated that Ni(II) binding did not saturate at 1 equivalent Ni(II) (data not shown), consistent with the static titration. In an attempt to observe the initial binding phase the UV-region of the spectrum was explored. A distinct faster process was found to occur at 300 nm followed by a slow phase (Figure 4C). Rate constants for the fast (k_{1Ni}) and slow phase (k_{2Ni}) at 300 nm were obtained (Figure 4C and Table 2), with k_{2Ni} essentially equal to k_{Ni} determined for the formation of the 350 nm band (Table 2). In Figure 4C we show more clearly the transition monitored at 350 nm where a lag-phase is more easily discerned and is seen to occupy the duration of the time taken to complete the fast phase at 300 nm, implying that a sequential mechanism of Ni(II) binding is being observed. The rate constant for the fast process at 300 nm is also [Ni(II)] independent indicating that the second order binding of Ni(II) to WT CsoR occurs more rapidly and without spectroscopic signature in this spectral range. However, once bound the non-cognate Ni(II) rearranges into the final Ni(II)-CsoR complex with rates that are > 500 times slower than for its cognate metal, Cu(I). Using the fingerprint and H103A variants the kinetics of Ni(II) binding was further investigated. For the C104A variant the fast phase at 300 nm (k_{1Ni}) is essentially unperturbed (Figure 5A and Table 2). However, the slower phase (k_{2Ni}) is no longer detected as may have be expected based on the very small absorbance increase at 340 nm in the static spectrum with saturating

[Ni(II)]. In contrast, the C75A variant abolishes both the fast phase at 300 nm and the slower 350 nm phase (Figure 5B) and this is also the case for the H100A variant. The non-fingerprint variant H103A also shows a loss of the fast phase at 300 nm (Figure 5C), with the absorbance at 300 nm now showing a simple increase with the rate constant, k_{2Ni}, similar to that for the formation of the 350 nm band (Table 2). This strongly suggests that His103 is involved in the mechanism of Ni(II) binding and participating in the faster of the two observed steps.

Cu(I)/Ni(II) metal displacement studies

In the absence of cellular control mechanisms to regulate metallation, a metallo-protein or -enzyme will select a divalent metal ion with a ranked order of preference that follows the Irving-Williams series [25]. Therefore the most competitive divalent metal ions will occupy the metal binding site(s), occluding weaker binding ions. In this respect Cu(II) will outcompete Ni(II) based on their respective positions in the Irving-Williams series, and this is thought to be also the case for Cu(I). An important issue to resolve in the present study and to gain further mechanistic insight into metal ion binding to this CsoR, is to confirm that Cu(I) and Ni(II) occupy the same binding site. To address this the kinetics of metal ion displacement were monitored. Cu(I)-loaded CsoR was mixed under anaerobic conditions in the stopped-flow with excess Ni(II). No spectral changes (*i.e.* formation of a 350 nm band) assigned to Ni(II) binding were observed, indicating that Cu(I) is occupying the site where Ni(II) binds and is not displaced on addition of Ni(II). This finding is thus in keeping with their respective positions in the Irving-Williams series [25]. The reverse displacement experiments, whereby the protein is largely occupied by Ni(II) (2 Ni(II): 1 CsoR monomer) and the 350 nm band is developed was then mixed in the stopped-flow with excess Cu(I). This resulted in the bleaching of the 350 nm band in which the time course can be fitted to a triple exponential function (Figure 6A) to give the rates reported in Table 3. We assign these to the sequential displacement of Ni(II) from its ligand set and the subsequent substitution by Cu(I). Concomitantly, absorbance changes monitored at 250 nm (*i.e.* binding of Cu(I)) showed a small fast phase (assigned to a small fraction of a Ni(II) free protein) and two phases with rate constants close to the values of k_1 and k_2 seen at 350 nm (Table 3), confirming the displacement of Ni(II) from ligation at the same site as Cu(I) is binding. On mixing WT CsoR with a single Ni(II) equivalent bound (300 nm band developed but little

350 nm absorbance developed) with excess Cu(I) resulted in the rates for the transition at 250 nm being essentially as observed in the absence of Ni(II) (Table 3). These data together with the earlier kinetic and static experiments support the notion that Ni(II) has two binding sites; one that has identical amino acid coordination as the Cu(I) binding site and the second involving His103, a residue not involved in the mechanism of Cu(I) binding. His103 has been identified above as being important for the formation of the fast phase seen at 300 nm and its absence changes the mechanism of Ni(II) binding. Stoichiometric addition of Ni(II) to the H103A variant is sufficient to give almost full absorbance of the 350 nm band compared to WT, which upon mixing with excess Cu(I) perturbed the kinetics in a similar manner as observed when two equivalents of Ni(II) are loaded to the WT CsoR; *i.e.* the rate constants obtained from a triple exponential fit for the bleaching of the 350 nm band are very similar to those for the formation of the 250 nm band (Figure 6B and Table 3).

Mechanism of Cu(I) and Ni(II) binding to S. lividans CsoR

Within the framework of the kinetic and static spectroscopic data presented above, a mechanism which can provide a consistent picture for both Ni(II) and Cu(I) binding to *S. lividans* CsoR is depicted in the scheme presented in Figure 7.

To account for the absence of a step, the rate of which is either [Cu(I)] or [Ni(II)] dependent, we propose that the metal ion binds rapidly to species (A) to form species (B), a complex that is spectroscopically silent in the spectral range monitored. Based on known metal-ligand preferences in model peptides [26-28] and supported by our spectroscopic data we suggest that Ni(II) binds initially to His103. Similarly, it is feasible that Cu(I) favours a Cys residue. This could be Cys75' as this makes a relatively small absorbance contribution in so far as the full absorbance change at 250 nm is observed in its absence (Table 1). However, we do not favour this explanation, as this is not consistent with displacement studies (*vide infra*) and we therefore suggest initial Cu(I) binding occurs at a site with ligands unknown at present, and other than those depicted in species (A).

The Ni(II)-adduct formed in species (B) rearranges to form species (C) whereby the His103 ligation remains intact and further ligation by way of Cys75' and His100 occurs, which gives rise to the absorbance at 300 nm. Species (C) rearranges such that His103 is displaced from coordination and Cys104 takes its place to form species (D). This reorganization is driven by binding a second Ni(II) to the freed

His103, thus accounting for the stoichiometric of binding observed in the static titration and the full formation of the 340 nm band. The rate constant (k_{2Ni}) for the transition between species (C) and (D) (Table 2), is most simply interpreted as the rate of His103 dissociation from Ni(II) in species (C). To account for the observation of the weak absorption transition at 480 nm, we include an unknown ligand, L, to give a favoured square planar Ni(II) geometry in the final Ni(II)-complex (species (D)).

Whereas His103 plays a key role in the mechanism of Ni(II) binding it appears to have no role in Cu(I) binding. Rather the encounter complex, species (B), with unknown Cu(I) coordination is rapidly transformed to species (E) in which Cu(I) coordinates to Cys104, the Cys residue that provides the most contribution to the absorbance at 250 nm (Table 1). There after, rearrangement of the Cu(I) coordinated Cys104 brings the metal into full coordination leading to the final Cu(I) complex species (F). Species (F) and (D) both utilize the X-Y-Z fingerprint to bind the respective metal ion, thus the high affinity cognate Cu(I) once bound, cannot be displaced by Ni(II) (over the concentration explored in our experiments), whereas the Ni(II) may be displaced readily from this site by Cu(I) (species (H)) at rates we assign to Ni(II) dissociation from the X-Y-Z ligand set. This mechanism of Cu(I) binding is supported by studies of the displacement of Ni(II) from species (C) that shows that when a single Ni(II) is bound the initial phases of Cu(I) binding, monitored at 250 nm, are unperturbed. This is as expected for a model in which Cys104 remains free in species (C). Cu(I) binding to species (C) leads to the formation of species (G) which then converts to species (H) in which the Cu(I) occupies its normal binding site and the Ni(II) may remain coordinated to the His103.

Although not determined here, there is a possibility that on binding Ni(II) to His103 the highly conserved N-terminal tail residue His37 may also participate in metal coordination. Structural evidence indicates this tail to be dynamic in the apo-state of CsoR members [13, 14, 29], but has recently been shown that upon binding Cu(I) this region becomes folded and lies over the Cu(I) binding site [14]. It is therefore conceivable that for Ni(II) binding, the tail may assist in the formation of the initial spectroscopically silent encounter complex (species (B)) enhancing the stabilization of this Ni(II)-adduct and also in species (D).

CONCLUSIONS

For Cu(I) binding to *S. lividans* CsoR the mechanism elucidated from the kinetic data is consistent with Cys104 (Z of the X-Y-Z fingerprint) having a primary role in the initial and final Cu(I) complex despite a lower affinity for Cu(I) than Cys75' (X of the X-Y-Z fingerprint). For Ni(II) binding the non X-Y-Z fingerprint residue, His103, plays a key role in initial binding proceeded by a ligand switching event between His103 and Cys104, that enables for the final complex to be formed and a second Ni(II) ion to bind. The ligand switching between His103 and Cys104 determined here through kinetic analysis is fully consistent with recent structural data reporting a 'quasi Cu(I)-bound' state of *S. lividans* CsoR, whereby conformational switching between the apo- and 'quasi Cu(I)-bound' states causes the Cys104 to move into the Cu(I) coordination sphere and the His103 to move away [30]. This in turn causes significant disruption to local secondary structure at the C-terminal ends of the α2-helices distorting the homotetramer and resulting in reorganization of surface charge distribution and the likely disassembly of the DNA bound complex [30]. From a biological perspective it is important to consider that Cu and Ni ions in the cell are likely to be at best partially hydrated. Cellular metal ions are 'buffered' at set levels and are coordinated to proteins e.g. metallochaperones or through a polydisperse pool of small organic molecules [5, 31]. Thus metal trafficking likely involves ligand-exchange type mechanisms. In *S. lividans* we have proposed a model in which the CsoR is loaded with Cu(I) by a CopZ metallochaperone [21]. CopZs have Cys residues in a Cu(I) binding motif (MXCXXC) with acid-base properties that are modulated for high cuprous ion affinity and favourable Cu(I)-exchange with a target [21]. The mechanism presented in this study with fully hydrated Cu (I) would suggest that in the transiently formed CopZ-Cu(I)-CsoR complex the Cys104 of CsoR is the initial attack ligand in a ligand-exchange type mechanism which results in Cu(I) being transferred in a unidirectional manner to the CsoR and subsequent derepression of the DNA operator. While displacement studies reveal that Cu(I) will always bind to the X-Y-Z fingerprint, *S. lividans* CsoR is capable of binding a Ni(II) ion equivalent via His103 when Cu(I) is bound at the X-Y-Z fingerprint. A His at this position is relatively well conserved across all Cu(I)-sensing CsoRs and may hint at the possibility that despite being allosterically specific for Cu(I), some CsoRs may have a non-allosteric secondary role involving the sequestering of metal ions during metal induced cell stress.

ACKNOWLEDGEMENTS

Financial support for this work was provided from the University of Essex.

REFERENCES

1. T. V. O'Halloran, *Science*, 1993, **261**, 715-725.
2. D. P. Giedroc and A. I. Arunkumar, *Dalton Trans*, 2007, 3107-3120.
3. Z. Ma, F. E. Jacobsen and D. P. Giedroc, *Chem Rev*, 2009, **109**, 4644-4681.
4. K. J. Waldron, J. C. Rutherford, D. Ford and N. J. Robinson, *Nature*, 2009, **460**, 823-830.
5. A. W. Foster, D. Osman and N. J. Robinson, *J Biol Chem*, 2014, **289**, 28095-28103.
6. A. Rodrigue, G. Effantin and M. A. Mandrand-Berthelot, *J Bacteriol*, 2005, **187**, 2912-2916.
7. J. S. Iwig, J. L. Rowe and P. T. Chivers, *Mol Microbiol*, 2006, **62**, 252-262.
8. J. S. Iwig, S. Leitch, R. W. Herbst, M. J. Maroney and P. T. Chivers, *J Am Chem Soc*, 2008, **130**, 7592-7606.
9. M. Garcia-Dominguez, L. Lopez-Maury, F. J. Florencio and J. C. Reyes, *J Bacteriol*, 2000, **182**, 1507-1514.
10. A. W. Foster, C. J. Patterson, R. Pernil, C. R. Hess and N. J. Robinson, *J Biol Chem*, 2012, **287**, 12142-12151.
11. T. Liu, A. Ramesh, Z. Ma, S. K. Ward, L. Zhang, G. N. George, A. M. Talaat, J. C. Sacchettini and D. P. Giedroc, *Nat Chem Biol*, 2007, **3**, 60-68.
12. K. Sakamoto, Y. Agari, K. Agari, S. Kuramitsu and A. Shinkai, *Microbiology*, 2010, **156**, 1993-2005.
13. S. Dwarakanath, A. K. Chaplin, M. A. Hough, S. Rigali, E. Vijgenboom and J. A. Worrall, *J Biol Chem*, 2012, **287**, 17833-17847.
14. F. M. Chang, H. J. Coyne, C. Cubillas, P. Vinuesa, X. Fang, Z. Ma, D. Ma, J. D. Helmann, A. Garcia-de los Santos, Y. X. Wang, C. E. Dann, 3rd and D. P. Giedroc, *J Biol Chem*, 2014, **289**, 19204-19217.
15. N. Grossoehme, T. E. Kehl-Fie, Z. Ma, K. W. Adams, D. M. Cowart, R. A. Scott, E. P. Skaar and D. P. Giedroc, *J Biol Chem*, 2011, **286**, 13522-13531.
16. J. L. Luebke, R. J. Arnold and D. P. Giedroc, *Metallomics : integrated biometal science*, 2013, **5**, 335-342.
17. J. L. Luebke, J. Shen, K. E. Bruce, T. E. Kehl-Fie, H. Peng, E. P. Skaar and D. P. Giedroc, *Mol Microbiol*, 2014, **94**, 1343-1360.
18. A. W. Foster, R. Pernil, C. J. Patterson and N. J. Robinson, *Mol Microbiol*, 2014, **92**, 797-812.
19. K. A. Higgins, P. T. Chivers and M. J. Maroney, *J Am Chem Soc*, 2012, **134**, 7081-7093.
20. Z. Ma, D. M. Cowart, R. A. Scott and D. P. Giedroc, *Biochemistry*, 2009, **48**, 3325-3334.
21. A. K. Chaplin, B. G. Tan, E. Vijgenboom and J. A. Worrall, *Metallomics : integrated biometal science*, 2015, **7**, 145-155.
22. G. L. Ellman, *Arch Biochem Biophys*, 1959, **82**, 70-77.
23. Z. Xiao, P. S. Donnelly, M. Zimmermann and A. G. Wedd, *Inorg Chem*, 2008, **47**, 4338-4347.

24. H. bateman, *Proceedings of ths Cambridge Philosophical Society, Mathematics and physical sciences*, 1910, **15**, 423-427.
25. H. Irving and R. J. Williams, *Nature*, 1948, **162**, 746-747.
26. D. Witkowska, R. Politano, M. Rowinska-Zyrek, R. Guerrini, M. Remelli and H. Kozlowski, *Chemistry-a European Journal*, 2012, **18**, 11088-11099.
27. D. Witkowska, M. Rowinska-Zyrek, G. Valensin and H. Kozlowski, *Coordination Chemistry Reviews*, 2012, **256**, 133-148.
28. D. Witkowska, D. Valensin, M. Rowinska-Zyrek, A. Karafova, W. Kamysz and H. Kozlowski, *Journal of inorganic biochemistry*, 2012, **107**, 73-81.
29. H. J. Coyne, 3rd and D. P. Giedroc, *Biomolecular NMR assignments*, 2013, **7**, 279-283.
30. T. V. Porto, M. A. Hough and J. A. Worrall, *Acta crystallographica. Section D, Biological crystallography*, 2015, **71**, 1872-1878.
31. K. J. Waldron and N. J. Robinson, *Nature reviews. Microbiology*, 2009, **7**, 25-35.

Table 1: Stopped-flow determined average pseudo first-order rate constants and amplitude change at 250 nm (Δε) for Cu(I) binding to *S. lividans* CsoR (10 μM) and mutants (20 ^{o}C, pH 7.4). Standard errors are given in parenthesis.

CsoR	k_{1Cu} (s^{-1})	k_{2Cu} (s^{-1})	k_{3Cu} (s^{-1})	Δε $M^{-1}cm^{-1}$
WT	312.6 (15.3)	38.7 (4.0)	2.3 (0.6)	10^4
H103A	312.8 (15.7)	53.2 (8.8)	4.4 (1.4)	1.1 x 10^4
C75A	320.6 (40.5)	62.4 (10.0)	9.8 (3.7)	9 x 10^3
H100A	249.4 (32.0)	22.8 (4.4)	1.3 (0.4)	6 x 10^3
C104A	367.6 (40.0)	35.3 (4.5)	2.5 (0.71)	3.5 x10^3

Table 2: Stopped-flow determined average pseudo first-order rates constants for Ni(II) binding to *S. lividans* CsoR (10 μM) and variants (20 ^{o}C, pH 7.4). Standard errors are given in parenthesis.

CsoR[a]	k_{Ni} 350 nm (s^{-1})	k_{1Ni} 300 nm (s^{-1})	k_{2Ni} 300 nm (s^{-1})
WT	0.072 (0.006)	0.65 (0.04)	0.10 (0.02)
H103A	0.083 (0.02)	-	0.09 (0.02)
C104A	-	0.97 (0.12)	-

[a]No rates were determined for the C75A and H100A variants as no spectral change was observed for.

Table 3: Stopped-flow determined pseudo first-order rate constants for the displacement of Ni(II) from WT and the H103A variant of *S. lividans* CsoR with Cu(I) (20 ^{o}C, pH 7.4). Standard errors are given in parenthesis.

	Bleaching of 350 nm band			Formation of 250 nm band		
Reaction	k_1 (s^{-1})	k_2 (s^{-1})	k_3 (s^{-1})	k_1 (s^{-1})	k_2 (s^{-1})	k_3 (s^{-1})
2 Ni(II)-CsoR + Cu(I)	90.9 (8.0)	3.5 (0.5)	0.6 (0.02)	553 (156)	66 (10.7)	10 (2.3)
1 Ni(II)-CsoR + Cu(I)[a]	-	-	-	391 (85)	25.4 (8.3)	-
1 Ni(II)-H103A + Cu(I)	62 (12)	7.9 (1.5)	1.14 (0.52)	89 (15)	7.3 (2.3)	0.8 (0.1)

[a]At 1 equivalent of Ni(II) the 350 nm band is not formed and the formation of the 250 nm band fitted adequately to a double exponential.

FIGURE LEGENDS

Figure 1: Structural and metal binding features of *Streptomyces lividans* CsoR. A) Tetrameric assembly of the apo-form determined from crystals grown at pH 4 [13]. Each protomer of the assembly is individually coloured and the helices of one protomer labeled. B) A close-up a Cu(I)-binding site indicated by the dashed circle in (A). In this apo-CsoR structure [13] the Cys104 Cu(I)-ligand is too far away from the other Cu(I)-ligands, Cys75' and H100 to create a pre-formed site. The position of His103 relative to the Cu(I)-ligands is indicated. C) Residues in the W-X-Y-Z fingerprint motif of CsoR/RcnR family members.

Figure 2: Stopped-flow kinetics of Cu(I) binding to *S. lividans* CsoR. A) Representative time courses monitored at 250 nm for WT CsoR (10 μM monomer) at increasing Cu(I) concentrations. Fits to the data points are indicated with the solid line. The break in the x-axis at 0.1 s enables for the end point absorbance to be observed. Total amplitude change at 250 nm derived from the kinetic data plotted as a function of the [Cu(I)]/[CsoR monomer] for WT CsoR (B) and the C75A fingerprint variant (C). The inset in (C) shows a fit (R^2 = 0.99) to the normalised amplitude change at 250 nm to yield a dissociation constant for Cu(I) binding.

Figure 3: Spectroscopic and regulatory properties of Ni(II) binding to *S. lividans* CsoR. A) Changes in the apo-CsoR base-lined absorption spectra (20 μM CsoR monomer) of A) WT and B) the H100A fingerprint variant upon increasing Ni(II) concentration. The inset in (A) reports the binding isotherm generated from the ΔAbs at 340 nm as a function of Ni(II) concentration. C) EMSA of WT CsoR and the *csoR* operator DNA sequence in the presence and absence of either Cu(I) and Ni(II).

Figure 4: Stopped-flow kinetics of Ni(II) binding to *S. lividans* WT CsoR. A) Spectra constructed at the following times, 6.5, 13, 18.5, 25, 35, 98 s, after mixing from the time courses at the indicated wavelengths shown in B) on reacting 10 μM of CsoR with 100 μM of Ni(II). The solid lines in (B) represent a monophasic fit to the data excluding the initial 5 s as discussed in the main text. C) Overlay of representative time courses collected at 300 and 350 nm with the solid line a fit to a double exponential function to give $k_{1Ni} = 0.56\ s^{-1}$ and $k_{2Ni} = 0.074\ s^{-1}$.

Figure 5: Stopped-flow kinetics of Ni(II) binding to *S. lividans* CsoR variants (10 μM). Representative time courses for A) C104A monitored at 300 nm, 100 μM Ni(II) B) C75A, 800 μM Ni(II) and C) H103A, 100 μM Ni(II). The solid lines through the time course data for the C104A and H103A variants are the fits to a single exponential function.

Figure 6: Stopped-flow displacement traces. A) Time courses at 350 and 250 nm (inset) of Cu(I) binding to WT *S. lividans* CsoR with two equivalents of Ni(II) bound. B) Time courses at 350 and 250 nm (inset) of Cu(I) binding to the H103A variant of *S. lividans* CsoR with one equivalent of Ni(II) bound. The red lines are representative of the fits to the data points as described in the text.

Figure 7: Mechanism of Cu(I) and Ni(II) binding to *S. lividans* CsoR. The possibility of a role for the N-terminal tail residue His37 in Ni(II) binding as discussed in the text is indicated in grey.

A

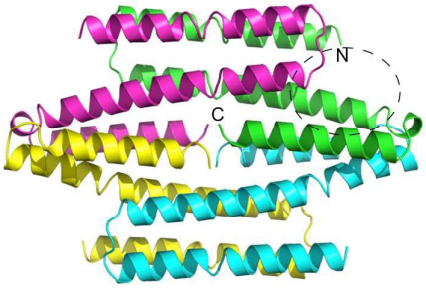

B

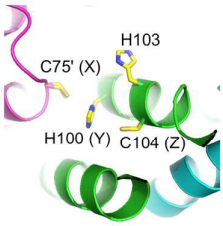

C

	W	X	Y	Z
CsoR	-	C	H	C
RcnR	H	C	H	H
InrS	H	C	H	C
CstR	-	C	-	C

Figure 1

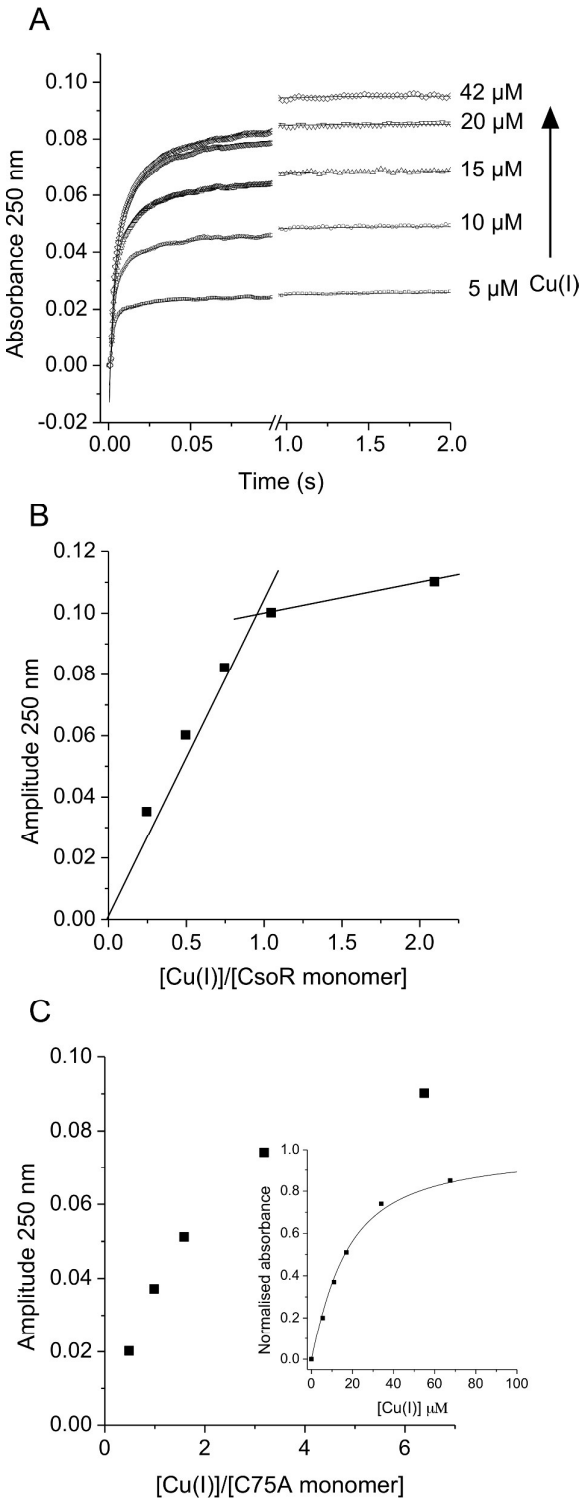

Figure 2

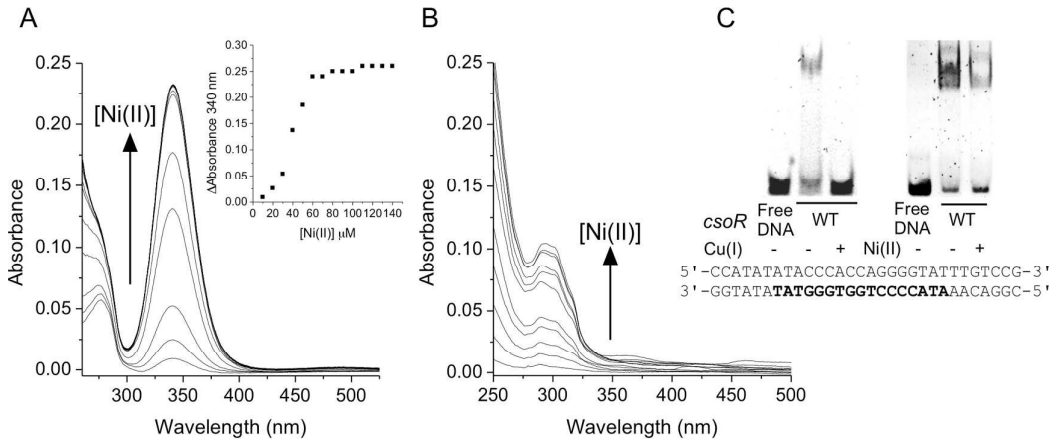

Figure 3

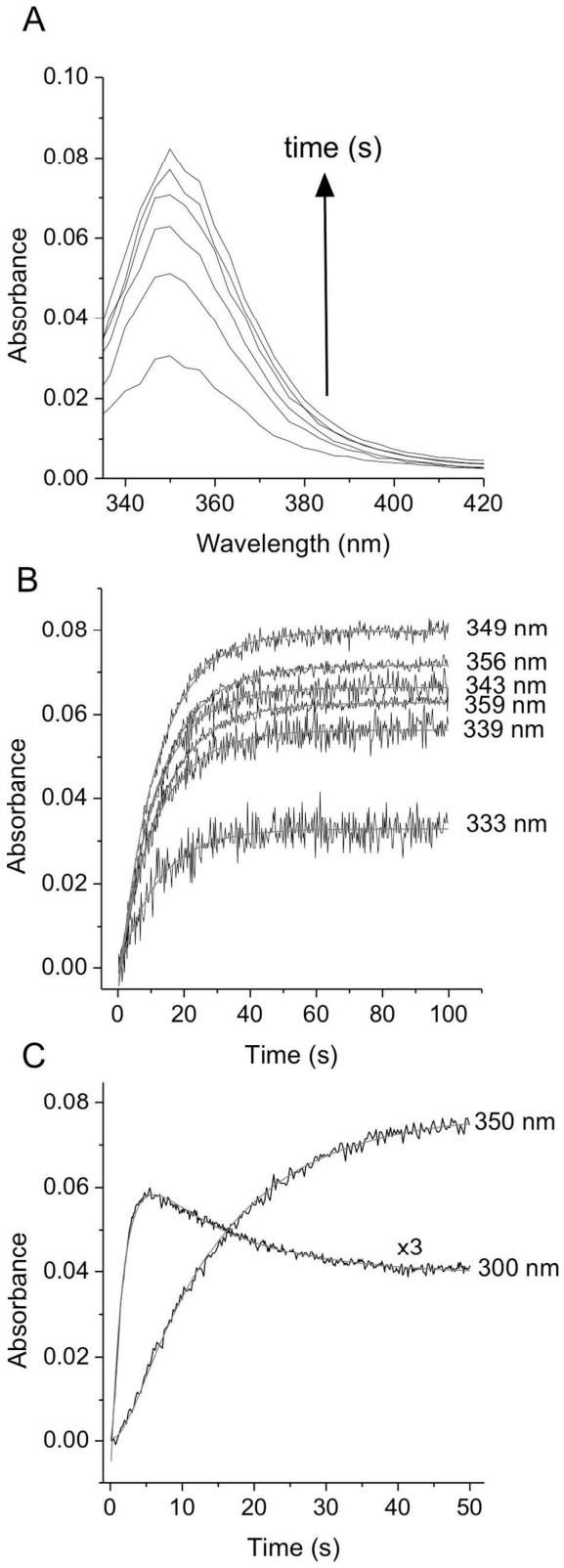

Figure 4

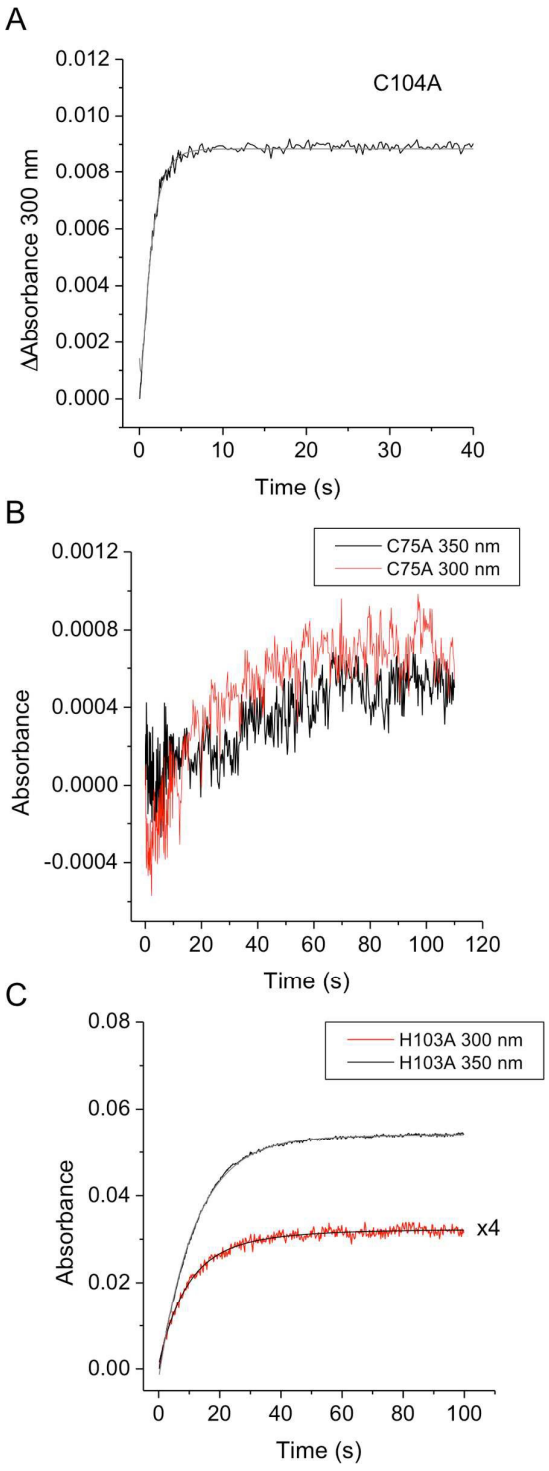

Figure 5

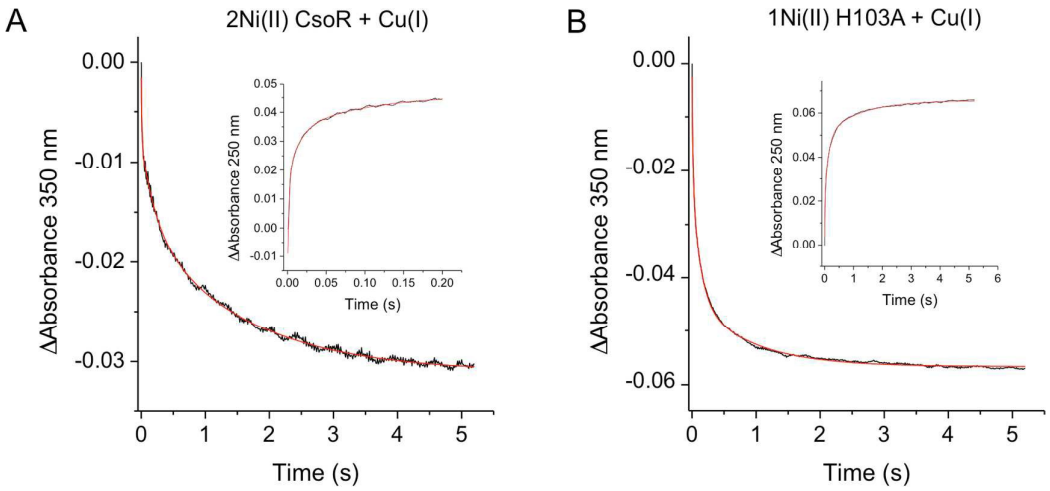

Figure 6

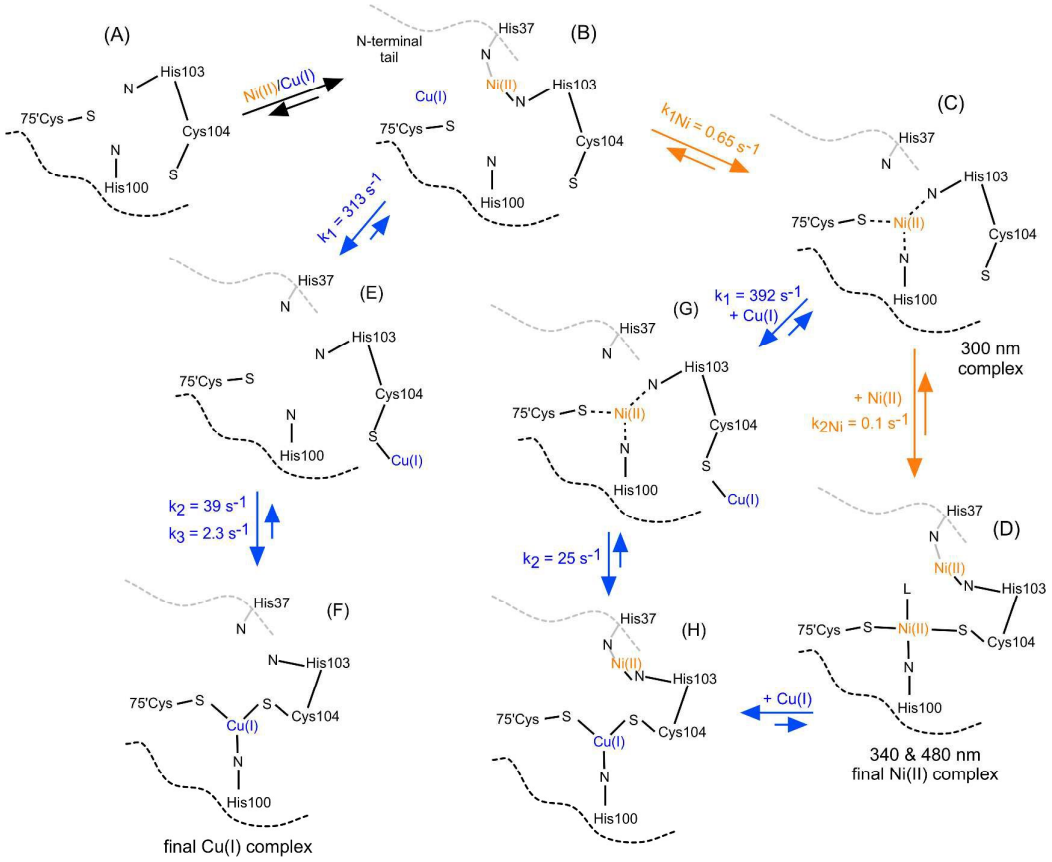

Figure 7